KnE Engineering

JICOMS
Jakarta International Conference on Multidisciplinary Studies towards Creative Industries
Volume 2024

Knowledge E
enriching | engaging | empowering

Research Article

New Design PdNi Heterogeneous Nanocatalysts for the Direct Synthesis of Hydrogen Peroxide

Tan-Thanh Huynh[1]*, Thi Tran Anh Tuan[2], Mawan Nugraha[3]

[1]School of Applied Chemistry, Tra Vinh University Tra Vinh, 8700, Viet Nam.
[2]School of Basic Sciences, Tra Vinh University Tra Vinh, 8700, Viet Nam.
[3]Teknik Grafika, Politeknik Negeri Media Kreatif, Indonesia

Abstract.

Hydrogen peroxide (H_2O_2) is a widely used chemical as an eco-friendly oxidizing agent, with water being the only byproduct of oxidation in applications like bleaching pulp and paper, making electronic semiconductors, chemical and detergent synthesis, and wastewater treatment. The direct synthesis approach is preferred to provide the environmentally friendly production of H_2O_2 for market requirements. Bimetallic PdNi nanocatalysts were chosen for this study because of their catalytic activity and the structural characteristics of the material system. First, for the development of order-structured bimetallic PdNi nanocatalysts based on mesoporous carbon template after hydrogen-assisted heat treatment at 750°C. The transformation of the disordered structure into ordered intermetallically structured PdNi alloys with higher alloying extents was confirmed by X-ray absorption spectroscopy (XAS) and high-resolution transition electron microscopy (HR-TEM). Then, to improve the oxygen oxidation reaction, two-electron pathway selectivity was used by TiO_2-C as a support-ordered structure material to facilitate strong metal-support interactions. XAS and X-ray photoelectron spectra (XPS) techniques show more clear evidence of metal-support interactions with electron transfer from defects in the TiO_2-C support to the ordered alloyed PdNi nanocatalysts, resulting in record productivity and selectivity of H_2O_2 production at ambient conditions. The results demonstrated in this study will enlighten a reliable design of new heterogeneous nanocatalysts with ordered structure. Electron transfer between hybrid support and active sites can clarify the catalytic behavior and prompt further research during the direct synthesis of hydrogen peroxide.

Keywords: hydrogen peroxide, direct synthesis, heterogeneous nanocatalysts PdNi, TiO_2-C

Corresponding Author:
Tan-Thanh Huynh; email:
htthanh@tvu.edu.vn

Published 7 March 2024

Publishing services provided by Knowledge E

Selection and Peer-review under the responsibility of the JICOMS Conference Committee.

1. INTRODUCTION

Hydrogen peroxide (H_2O_2) is an inorganic oxidant agent. H_2O_2 is a kind of colorless liquid, which is more viscous than water. It is easy to decompose by exposure to daylight and soluble in water, alcohol due to intermolecular hydrogen bonding. H_2O_2 was first discovered by Louis Jacques Thénard in 1818 as the product by hydrolysis of barium oxide and sulfuric acid solution. Up to now, it has become one of the most-100 important chemical in the world [1]. Currently, more than 95% of the world's H_2O_2 is produced by anthraquinone oxidation (AO) as depicted in the flow chart below:

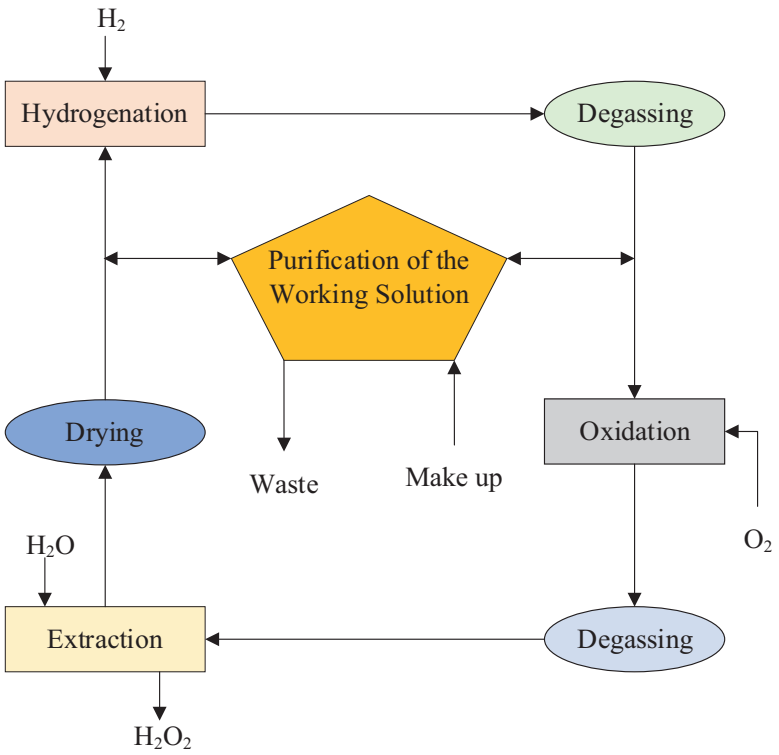

Figure 1: The anthraquinone process for hydrogen peroxide manufacture.

However, the anthraquinone process is not considered a green process as it requires significant energy input and generates waste; thus, it is not a suitable for the environmentally friendly synthesis of H_2O_2.

H_2O_2 is a highly effective, green, and selective oxidant for many oxidation reactions. The oxidation process of hydrogen peroxide is an environment friendly oxidation that has many benefits since the oxidation product contains only water [2]. Challenges related to the direct synthesis of H_2O_2 are generally related to catalyst selectivity. Pd is a popularly used catalyst for the direct synthesis of hydrogen peroxide, due to its high selectivity and yield, factors that are reflected in both computational and experimental studies [3-5].

Therefore, an ideal catalytic performance should achieve both enhanced selectivity and reduced H_2O_2 degradation. The synthesis the hybrid support TiO_2-C to the ordered alloy PdNi can clarify enhance productivity and selectivity up to 83.3 mole.kg^{-1}.h^{-1} and 96.15%, respectively.

METHODOLOGY AND MATERIALS

1.1. Catalyst preparation

The ordered alloy PdNi nanocatalysts were precepitated on mesoporous silica (SBA-15) by the wet impregnation method to form a smooth gel that reported by T-T Huynh et al [6]. Then, titanium isopropoxide (Sigma-Aldrich) as TiO_2 source was added before the smooth dispersion gel was aged in flowing air, as illustrated in Fig. 2. The gel was was thermo-treated at 750 ˚C in Ar with a flow rate of 5 ºC.min^{-1} for 4 hours. The product was divided into two parts; one part was further calcined in 5%H_2/Ar at 750 ºC for 4 hours. Finally, the both were dispersed in a NaOH 4M to remove the template. Then the resulting solid was filter by centrifuge.

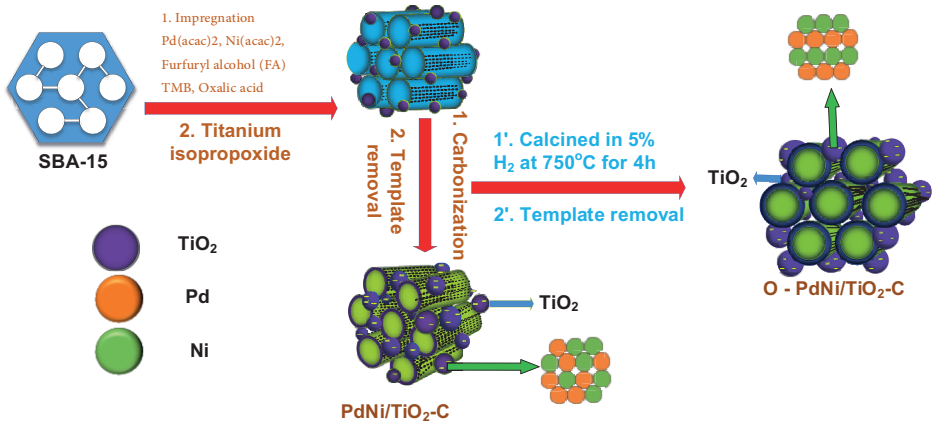

Figure 2: Scheme for the preparation of O-PdNi/TiO_2-C, and PdNi/TiO_2-C catalysts.

1.2. Catalyst characterizations

Scanning electron microscopy (SEM) and X-ray diffraction (XRD) were used to characterize the morphology of the hybrid supports i.e. TiO_2-C and the PdNi alloyed NPs. High-quality SEM images were obtained using field emission scanning electron microscopy (FESEM), JSM-7001F with an accelerating voltage of 30 kV, and Energy-dispersive X-ray spectroscopic (EDS) measurements were made for metal dispersion characterizations on the catalyst's surface. The X-ray diffraction patterns of the PdNi alloy and O-PdNi

alloy nanocatalysts were collected using a D2 phaser diffractometer (2θ range from 15° to 85°, scan rate 0.1 deg. s^{-1}) to determine their structural and lattice parameters. Transmission electron microscopy (FEI Tecnai G^2 FE-TEM) with an accelerating voltage of 200 kV was used to verify the particle size and superlattice interplanar distances. X-ray photoelectron spectra (XPS) were taken to determine the binding energy shifts in the TiO_2-C of hybrid support. X-ray absorption spectra (XAS) were measured at room temperature with solid samples. Pd foil, Ni foil, TiO_2 rutile, and TiO_2 anatase were used as references for the Pd L-, and K-edge, Ni L-, and K-edge, and Ti L and K-edge. The XAS technique was use to determine alloyed extent.

1.2.1. Catalyst activity

This research was used a common method to determine hydrogen peroxide production by using permanganate titration in a solution. The other was prepared using deuterium oxide [D_2O, (50 mL), 99.9%D, (Sigma Aldrich)] to allow for ^1H NMR measurements to calculating selectivity. All measurements were conducted by first purging the reactor with Ar, followed by feeding-in 5% H_2/Ar and O_2 (1:1) at room temperature.

2. RESULTS AND DISCUSSION

2.1. Catalyst characterizations

The catalysts' structures and morphologies were confirmed by XRD and Scanning electron microscopy (SEM), as shown in Fig. 3. The XRD patterns of all samples have a significant shift diffraction peak (111) between Pd (05-0683) and Ni (04-0850), which originates in the crystal structure of the Pd and Ni alloy Fig. 3(a) - with O-PdNi/TiO_2-C and O-PdNi/C XRD, the patterns show the main diffraction peak (111) to be between 40° and 45°. In addition, O-PdNi/TiO_2-C has an overlapping peak at ~41°, which is attributed to the TiO_2 crystal diffraction peak. The average crystallite size of PdNi nanocatalysts was calculated, from the diffraction line of the broadening peak (111), to be ~6 nm, using the Scherrer equation. The elemental composition was estimated by energy-dispersive spectroscopy (EDS). As shown in Figs. 3(c)-(d), the catalysts have similar morphologies on the surfaces of C and on the TiO_2-C hybrid support.

Fig. 4 shows high-resolution transition electron microscopy (HR-TEM) and high angle annular dark-field (HAADF) images of the best performing catalyst, *i.e.* O-PdNi/TiO_2-C. As can be seen, the alloyed PdNi catalyst's particle size was ~5 nm in Fig. 4(a). Selective

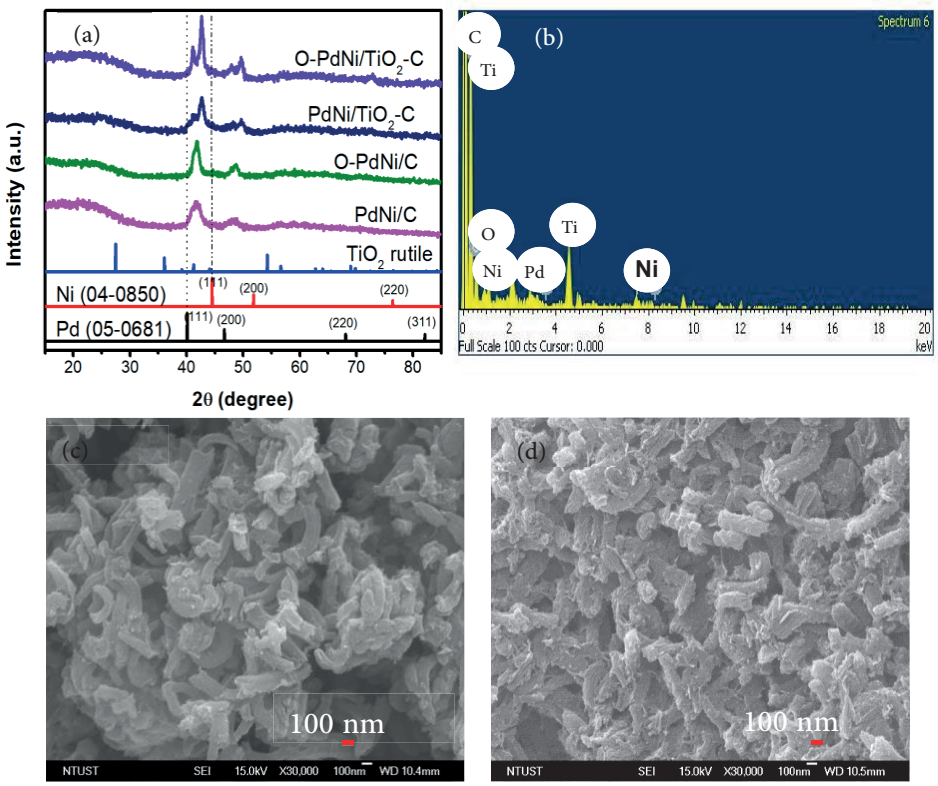

Figure 3: (a) XRD patterns of PdNi/C, O-PdNi/C, PdNi/TiO_2-C, O-PdNi/TiO_2-C catalyst. (b) EDS spectrum of O-PdNi/TiO_2-C. (c), and (d) SEM images of O-PdNi/C, and O-PdNi/TiO_2-C, respectively.

area electron diffraction (SAED) was used to show the catalyst's interplanar distances and the formation of the PdNi crystalline alloy. The Bragg diffraction fringes are diffused, due to PdNi crystal size being small (inset in Fig. 4(a)). The ordered phase of the PdNi alloy was identified as the superlattice structure using the Fast Fourier Transformation (FFT) filter function, see the rings of corresponding to (001) and (110) in the inset of Fig. 4(b). The lattice spacings of 2.17Å, 1.89Å, and 1.35Å, corresponding to the (111), (200), and (220) planes, are clearly seen in Fig. 4(c), which provide reliable evidence for ordered PdNi alloy formation after hydrogen treatment at high temperature. The above results, shows well-dispersed PdNi alloy nanoparticles with similar sizes on the hybrid support.

The surface composition and the chemical state of the elements in both the TiO_2-C support and in O-PdNi/TiO_2-C were studied by XPS. High-resolution C 1s, O 1s, and Ti 2p spectra were measured. As seen in Fig. 5(a), the XPS spectra of C-C bonds was recorded at 284.8 eV in both TiO_2-C and O-PdNi/TiO_2-C, this being due to their high carbon contents, while in addition adventitious carbon C-O binding was found by at 288 eV. These results are in good agreement with the EDS composition analysis and the HR-TEM distribution mentioned in the above discussion. The presence of C-O binding was also confirmed by O 1s spectra, see Fig. 5(b). The main peak of O 1s should be

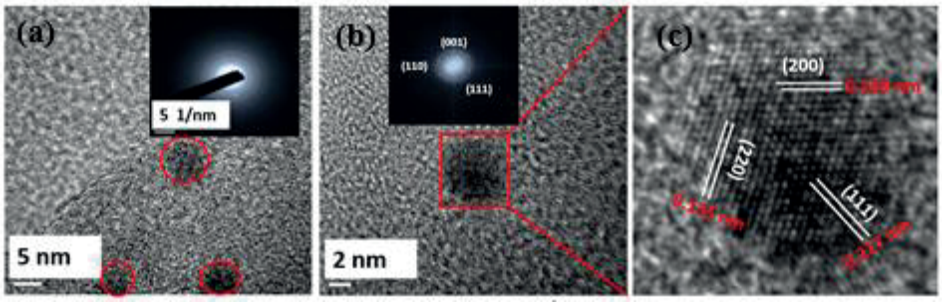

Figure 4: (a), (b) HR-TEM of O-PdNi/TiO_2-C, (c) with a magnified area taken from the red square. The corresponding SAED patterns and FFT of O-PdNi/TiO_2-C are shown in the insets of (a) and (b), respectively.

at 529 – 530 eV for O-Ti in TiO_2, however here the bonding peak is at 531.86 eV [7]. This binding energy shift in the O 1s spectra in TiO_2-C is ascribed to the C-O bonding. Furthermore, the position of the two peaks representing Ti 2p shown at 459.45 eV and 465.39 eV are the symmetric peaks of Ti $2p_{3/2}$ and Ti $2p_{1/2}$, respectively, as shown in Fig. 4(c). The splitting value ΔE binding energy is 5.8 eV between Ti $2p_{3/2}$ and Ti $2p_{1/2}$ and is due to the Ti^{4+} in the support [8]. The Ti $2p_{1/2}$ component was also found to be much broader than the Ti $2p_{3/2}$ peak. However, the spectra of Ti 2p after catalyst loading and high-temperature treatment was shifted to a lower binding energy (457.7 eV) leading to an increase in the Ti^{3+} oxidation state this being due to TiO_2 defects or oxygen vacancies formed on the surface of the hybrid support TiO_2-C [9]. The binding energy decreases after catalyst deposition, due to the addition of valence electron charge from the alloy catalyst to the defect containing support [10]. XPS spectra give strong evidence showing the presence of the Ti-O-C bonding and oxygen vacancies on the TiO_2 surface in the hybrid support. The results are indicative of strong metal-support interactions in heterogeneous catalysis.

The employed XAS to evaluate the electronic structures and valance states of various elements. Fig. 5(a) shows the X-ray absorption near edge structure (XANES) spectra of Ti K-edge of all the catalysts. Fig. 5(a1) shows the Ti pre-edge region of TiO_2-C in comparison with TiO_2 anatase, TiO_2 rutile, and PdNi/TiO_2-C, O-PdNi/TiO_2-C. The pre-edge peaks of the TiO_2 anatase and rutile phases were determined by the transition from the 1s to 3d molecular orbitals [11]. The pre-edge position shifted to a higher energy, while the prominent peak in TiO_2-C, without catalyst loading, indicated increased Ti coordination numbers, which agrees well with the XPS results. The intensity of the Ti pre-edge peak with catalyst loading was shown to be higher than without catalyst loading, due to the 'coordination chemistry' that exists with catalyst loading. The XANES spectrum of the TiO_2-C and catalysts in Fig. 5(a2) shows the edge-jump region. The

adsorption peak at ~4985 eV represents the electronic transition occurring in two the phases of TiO_2, and is included here as a reference. However, the adsorption peak of TiO_2-C in three samples shifted to a higher energy around 4990 eV, due to the changing coordination environment of the Ti metal and different interaction intensity resulting form interactions with alloyed PdNi [12]. As a result, Ti XANES of TiO_2-C shows that Ti is less positively charged than Ti XANES in O-PdNi/TiO_2-C, and PdNi/TiO_2-C. This value is due to the influence of the electron transfer between the hybrid support and the catalyst. The result also indicates that the bonding between Ti-O-C in the support is in accord with the XPS analysis. The EXAFS spectra clearly show the formation of Ti-O bonding at 1.7Å [13] and Ti-metal bonding at approximately 2.4 to 2.8Å in Fig. 5(b): note that the intensity found for catalytic TiO_2 is lower than that of all the references. This suggests a coordination number change around Ti with catalyst loading. Interestingly, the peak appearing at 1.1Å may be due to C-O bonding, see Fig. 5(b) [14].

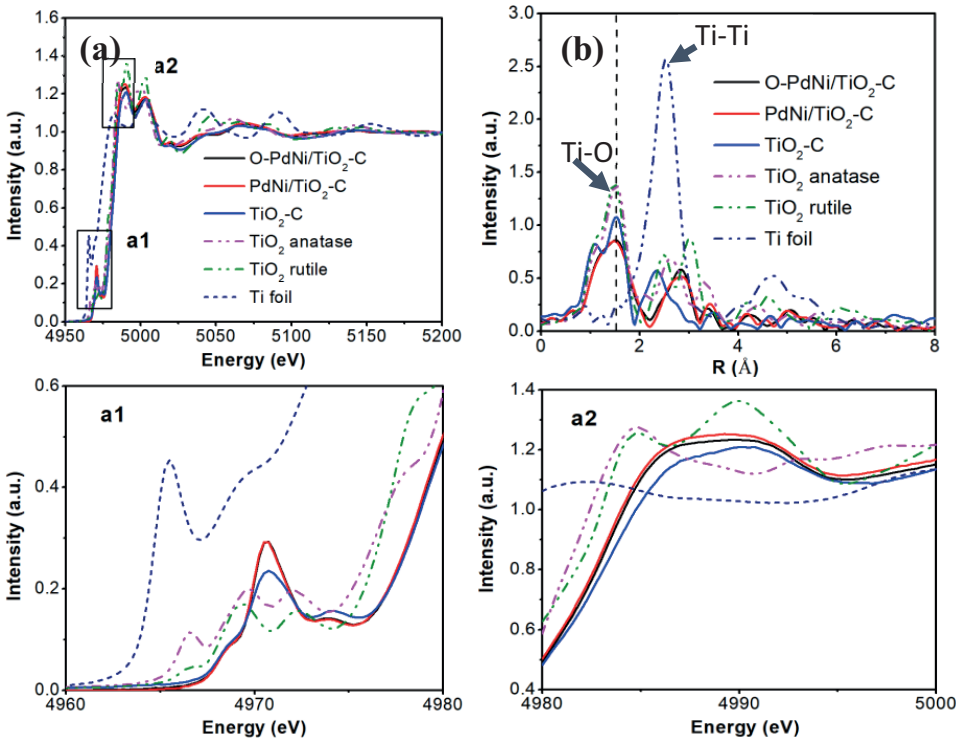

Figure 5: XANES spectra of Ti K-edge, (b) EXAFS spectra of TiO_2-C, PdNi/TiO_2-C and O-PdNi/TiO_2-C. a1) enlarged pre-edge features of Ti K-edge XANES spectra and a2) enlarged edge jump features of Ti K-edge XANES spectra.

To identify the synergistic effect existing between TiO_2-C and the PdNi alloy during H_2O_2 production, the Ti L-, Pd L-, and Ni L-edges were observed, see Fig. 6. The XANES white line Ti $L_{3,2}$-edge was observed to identify the electronic structure on the surface of hybrid support TiO_2-C in Fig. 6(a). The lower intensity of the Ti $L_{3,2}$-edge after catalyst

loading was due to strong coulombic interaction between the metal and Ti 3d empty states. As can be seen, the white line intensity of TiO_2-C (blue curve) is higher than that of TiO_2-C with the catalyst loading (red and black curve in Fig. 6(a)). This value confirmed that the TiO_2-C support had withdrawn electron density from the PdNi alloy, which can be regarded as a strong metal-support interaction (SMSI) [15, 16] between PdNi NPs and the TiO_2-C hybrid support. For low loadings of Pd and Ni metal, we used a silicon drift detector (SDD) to measure electron transfer in the catalyst. The white line intensities of the Pd L-edge and Ni L-edge in O-PdNi/TiO_2-C were higher than in PdNi/TiO_2-C, as shown in Fig. 6(b-c). It can be seen that the XANES white line of the Pd metal state peak appears at 3174 eV [17]. The white line intensity was determined by the degree of electronic transfer between the ordered structure of O-PdNi and the disordered PdNi catalyst to the hybrid support. The significantly higher intensity of Pd in the O-PdNi catalyst suggested stronger electronic transfer than in PdNi catalyst. Interestingly, Ni atom's oxidation state in the catalyst was shown to be in the region at 852 eV and 854 eV [18]. Similarly, the white line intensity of Ni in O-PdNi is significantly higher than that is in PdNi. The intensity changes not only confirm the presence of SMSI but also indicates electronic transfer between the catalyst and the support. This result is important with respect to achieving high selectivity for the oxygen reduction reaction two-electron pathway [19]. Therefore, we can say that the synergistic TiO_2-C hybrid support has an important role in the PdNi bimetallic catalyst towards H_2O_2 production, which is obviously not possible in a simple carbon support.

The synergistic effects of ordered structure catalysts towards the selectivity and production of H_2O_2 was examined using the XANES spectra of Pd and the Ni K-edge [6]. The XAS of Pd and Ni, see Fig. 7, show that Heterometallic bonding can enhance catalytic activity: Figs. 7(a)-(b) show the XANES spectra of Pd and the Ni K-edge, respectively. The position peak of Pd and the Ni K-edge are seen to show similar trends to the trends of Pd and Ni foil when used as comparative references. This indicates the presence of the metallic state of Pd and Ni in all the catalysts. Moreover, the white line peak was also observed with the Pd-Ni oxidation state in the catalysts, as shown by peaks shifts in the ordered structures [20], see the insets in Figs. 7(a)-(b). A comparison of the electronic interactions between Pd and Ni in ordered and disordered catalyst structures was undertaken by comparing the white line intensities. It was found the electronic effects in ordered structures were stronger than in disordered structures, due to the greater extent of alloying. EXAFS were studied to obtain the bond lengths and coordination numbers of bimetallic catalysts, see Figs. 7(c)-(d) of the Pd and Ni K-edges, respectively. In this case, the longest bond length is Pd-Pd (2.5 Å) in Pd foil, and the

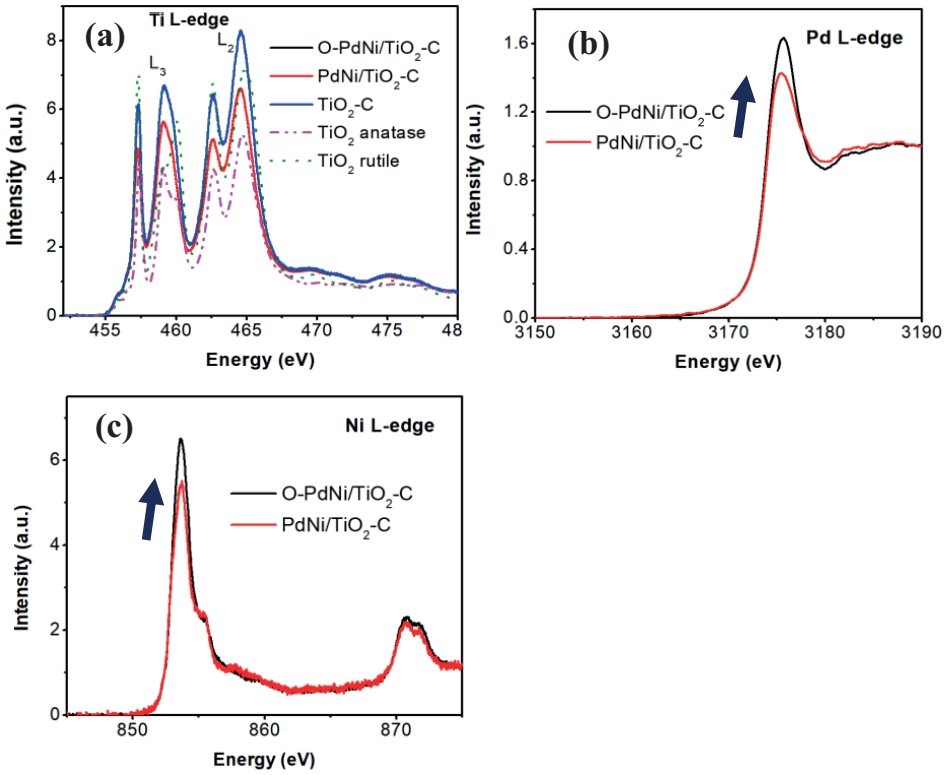

Figure 6: XANES spectra: (a) Ti L-edge, (b) Pd L-edge, (c) Ni L-edge of $PdNi/TiO_2$-C and O-$PdNi/TiO_2$-C.

shortest bond length Ni-Ni (2.2 Å) is in Ni foil. From the EXAFS of Pd, the bond lengths of Pd-Ni and Pd-Pd were found to be 2.2 Å and 2.4 Å, respectively, as shown in Fig. 7(c). The intensity in ordered structures, being higher than that in disordered alloys, indicates that the Ni atom offers a significant coordination contribution with Pd. In contrast, the EXAFS of Ni with a peak around 2.2 Å in Fig. 7(d) shows the Ni-Pd bonding contribution and the lower intensity in an ordered structure having high coordination with Pd.

The heterometallic bonding in ordered alloys and hybrid supports significantly enhanced the activity (83.3 $mole.kg^{-1}.h^{-1}$) and selectivity (96%) for the direct synthesis of hydrogen peroxide, especially with a reduced total metal loading (1.27 wt%). Our work is strongly conceptual and offers the first design of a new, highly selective, catalyst for the direct synthesis hydrogen peroxide.

3. CONCLUSION AND RECOMENDATION

On hybrid TiO_2-C supports, we have effectively created structurally ordered PdNi catalysts that exhibit distinct synergistic effects when applied to the direct generation of hydrogen peroxide. An efficient method for creating nanocatalysts for the direct

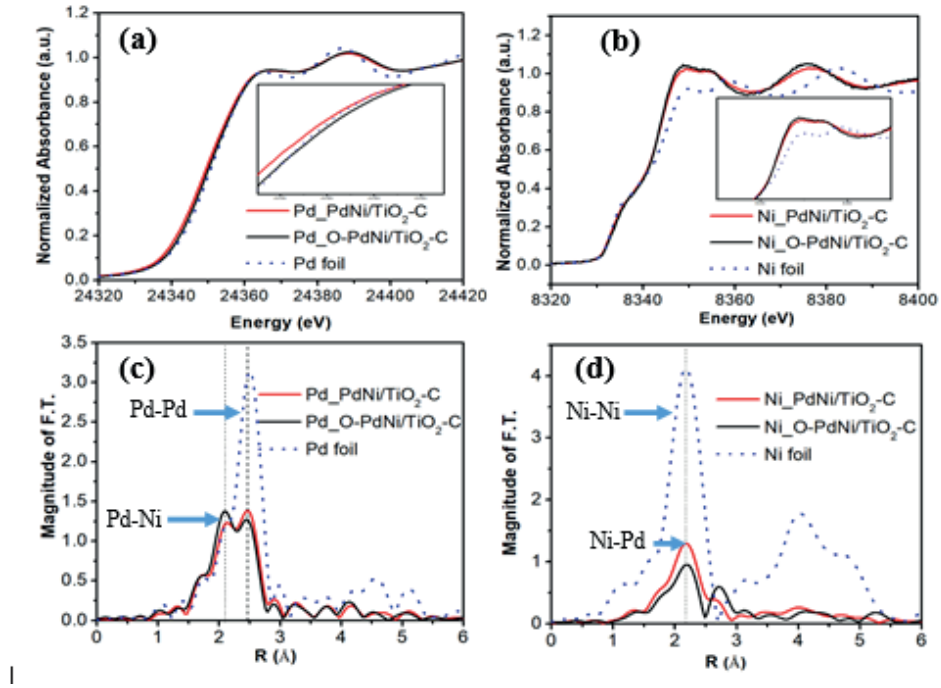

Figure 7: XANES spectra of: (a) Pd K-edge and (b) Ni K-edge; EXAFS spectra of (c) Pd, and (d) Ni in PdNi/TiO_2-C and O-PdNi/TiO2-C. Inset XANES edge jump of Pd and Ni.

manufacture of hydrogen peroxide has been found to be the use of earth-abundant Ni to create the PdNi nanocatalyst and the transformation of the nanoalloys into ordered structures. Stronger electronic interactions in catalysts with ordered structures lead to the high activity toward H_2O_2 production, whereas the hybrid TiO_2-C support is responsible for the increased selectivity. The activity and selectivity of O-PdNi/TiO_2-C are higher than those reported for Pd-based alloy catalysts in the literature. For the direct production of hydrogen peroxide, the heterometallic bonding in ordered alloys and hybrid supports dramatically increased activity (83.3 mole kg^{-1} h^{-1}) and selectivity (96%).

References

[1] Lewis RJ, Hutchings GJ. Recent Advances in the Direct Synthesis of H2O2. ChemCatChem. 2019;11:298–308.

[2] Puértolas B, Hill AK, García T, Solsona B, Torrente-Murciano L. In-situ synthesis of hydrogen peroxide in tandem with selective oxidation reactions: A mini-review. Catal Today. 2015;248:115–27.

[3] Tian P, Xu X, Ao C, Ding D, Li W, Si R, et al. Direct and Selective Synthesis of Hydrogen Peroxide over Palladium-Tellurium Catalysts at Ambient Pressure. ChemSusChem.

2017 Sep;10(17):3342–6.

[4] Seo Mg, Lee DW, Han SS, Lee KY. Direct Synthesis of Hydrogen Peroxide from Hydrogen and Oxygen over Mesoporous Silica-Shell-Coated, Palladium-Nanocrystal-Grafted SiO2 Nanobeads. ACS Catal. 2017;7:3039–48.

[5] Nugraha M, Tsai MC, Su WN, Chou HL, Hwang BJ. Descriptor study by density functional theory analysis for the direct synthesis of hydrogen peroxide using palladium–gold and palladium–mercury alloy catalysts. Mol Syst Des Eng. 2018;3:896–907.

[6] T.-T. Huynh, M.-C. Tsai, C.-J. Pan, W.-N. Su, T.-S. Chan, J.-F. Lee, B.-J.J.E.C. Hwang, Synergetic electrocatalytic activities towards hydrogen peroxide: Understanding the ordered structure of PdNi bimetallic nanocatalysts, 101 (2019) 93-98.

[7] Gu DE, Lu Y, Yang BC, Hu YD. Facile preparation of micro-mesoporous carbon-doped TiO2 photocatalysts with anatase crystalline walls under template-free condition. Chem Commun (Camb). 2008 Jun;(21):2453–5.

[8] Song Z, Hrbek J, Osgood R. Formation of TiO2 nanoparticles by reactive-layer-assisted deposition and characterization by XPS and STM. Nano Lett. 2005 Jul;5(7):1327–32.

[9] Pan X, Yang MQ, Fu X, Zhang N, Xu YJ. Defective TiO2 with oxygen vacancies: synthesis, properties and photocatalytic applications. Nanoscale. 2013 May;5(9):3601–14.

[10] C.-J. Pan, M.-C. Tsai, W.-N. Su, J. Rick, N.G. Akalework, A.K. Agegnehu, S.-Y. Cheng, B.-J.J.J.o.t.T.I.o.C.E. Hwang, Tuning/exploiting strong metal-support interaction (SMSI) in heterogeneous catalysis, 74 (2017) 154-186.

[11] T. Hiratoko, A. Yoshiasa, T. Nakatani, M. Okube, A. Nakatsuka, K.J.J.o.s.r. Sugiyama, Temperature dependence of pre-edge features in Ti K-edge XANES spectra for ATiO3 (A= Ca and Sr), A2TiO4 (A= Mg and Fe), TiO2 rutile and TiO2 anatase, 20 (2013) 641-643.

[12] F. Leitzke, R. Fonseca, J. Göttlicher, R. Steininger, S. Jahn, C. Prescher, M.J.C.t.M. Lagos, Petrology, Ti K-edge XANES study on the coordination number and oxidation state of Titanium in pyroxene, olivine, armalcolite, ilmenite, and silicate glass during mare basalt petrogenesis, 173 (2018) 1-17.

[13] D. Carta, G. Mountjoy, A. Regoutz, A. Khiat, A. Serb, T.J.T.J.o.P.C.C. Prodromakis, X-ray absorption spectroscopy study of TiO2–x thin films for memory applications, 119 (2015) 4362-4370.

[14] B. Yang, J. Kirz, T.J.P.R.A. Sham, Oxygen K-edge extended x-ray-absorption fine-structure studies of molecules containing oxygen and carbon atoms, 36 (1987) 4298.

[15] S. Tauster, S. Fung, R.L.J.J.o.t.A.C.S. Garten, Strong metal-support interactions. Group 8 noble metals supported on titanium dioxide, 100 (1978) 170-175.

[16] N.V. Krstajic, L.M. Vracar, V.R. Radmilovic, S.G. Neophytides, M. Labou, J.M. Jaksic, R. Tunold, P. Falaras, M.M.J.S.S. Jaksic, Advances in interactive supported electrocatalysts for hydrogen and oxygen electrode reactions, 601 (2007) 1949-1966.

[17] K.-i. Shimizu, Y. Kamiya, K. Osaki, H. Yoshida, A.J.C.S. Satsuma, Technology, The average Pd oxidation state in Pd/SiO 2 quantified by L 3-edge XANES analysis and its effects on catalytic activity for CO oxidation, 2 (2012) 767-772.

[18] D.-Y. Cho, S.J. Song, U.K. Kim, K.M. Kim, H.-K. Lee, C.S.J.J.o.M.C.C. Hwang, Spectroscopic investigation of the hole states in Ni-deficient NiO films, 1 (2013) 4334-4338.

[19] Jung E, Shin H, Lee BH, Efremov V, Lee S, Lee HS, et al. Atomic-level tuning of Co-N-C catalyst for high-performance electrochemical H_2O_2production. Nat Mater. 2020 Apr;19(4):436–42.

[20] E.-K. Hlil, R. Baudoing-Savois, B. Moraweck, A.J.T.J.o.P.C. Renouprez, X-ray absorption edges in platinum-based alloys. 2. Influence of ordering and of the nature of the second metal, 100 (1996) 3102-3107.